Bull. Mater. Sci. (2022) 45:189
https://doi.org/10.1007/s12034-022-02778-2

Differing pressure response of lattice structure in $LaTMSb_2$ (TM = Au or Ag) ternary antimonides

GOVINDARAJ LINGANNAN[1,2], BOBY JOSEPH[2], CHIA NUNG KUO[3,4], CHIN SHAN LUE[3,4], PONNIAH VAJEESTON[5] and ARUMUGAM SONACHALAM[1,*]

[1]Centre for High Pressure Research, School of Physics, Bharathidasan University, Tiruchirappalli 620024, India
[2]Elettra-Sincrotrone Trieste S.C. p. A., S.S. 14, Km 163.5 in Area Science Park, 34149 Basovizza, Italy
[3]Department of Physics, National Cheng Kung University, Tainan 70101, Taiwan
[4]Taiwan Consortium of Emergent Crystalline Materials, Ministry of Science and Technology, Tapei 10601, Taiwan
[5]Department of Chemistry, Centre for Materials Science and Nanotechnology, University of Oslo, Blindern, Oslo 0318, Norway
*Author for correspondence (sarumugam1963@yahoo.com)

MS received 4 May 2022; accepted 8 June 2022

Abstract. Ternary antimonides $LaTMSb_2$ (TM = Au or Ag) share identical lattice symmetry and exhibit the charge density wave (CDW) phenomenon. The CDW is found to be tunable either by physical or chemical pressure, triggering the investigation of the pressure response of these systems. Here, we compare the lattice structure response of the two systems to the hydrostatic pressure. Under hydrostatic pressure, the lattice structure of $LaAgSb_2$ transformed from tetragonal to a mixed tetragonal (>4 GPa) followed by monoclinic (4–9 GPa) and then to a mixed monoclinic and orthorhombic (9–41.8 GPa) phases. In contrast, our synchrotron X-ray diffraction results on $LaAuSb_2$ reveal that the tetragonal structure is stable in the pressure range of 0–12.2 GPa. Our experimental investigation is well supported by the density functional theory (DFT) calculations. We have used DFT to identify the experimental Raman vibrational modes at ambient conditions. We highlight the importance of structural subtleties in the differing pressure response of the ternary antimonides.

Keywords. Ternary antimonides; charge density wave; synchrotron powder XRD; hydrostatic high pressure; Raman.

1. Introduction

Ternary antimonides $RETMSb_2$ (RE = rare earth, TM = transition metal) are gaining popularity due to their exotic low temperature physical phenomena, such as charge density wave (CDW) [1,2], superconductivity (SC) [3], ferromagnetism [4], quantum critical point [5], etc. Among these, the sister compounds $LaAgSb_2$ and $LaAuSb_2$ crystallize in the $ZrCuSi_2$-type tetragonal structure (P4/nmm, No. 129). In these ternary antimonides, La and TM (Au or Ag) were separated by layers of Sb along the *c*-axis. These Sb layers form a square net structure and have got immense attraction as hosts of Dirac fermions [6]. $LaAgSb_2$ exhibits two CDW transitions at T_{CDW1} = 207 K and T_{CDW2} = 186 K. In this system, X-ray diffraction (XRD) revealed a CDW modulation with modulation wave vector approximately (0.026 0 0) evolved below 207 K, opening a gap in Fermi surface (FS). A second CDW modulation was also observed below 186 K in the out-of-plane direction (0 0 0.16) [2]. Further, a linear trend in the structural lattice parameters of $LaAgSb_2$ disclosed a clear change at 180 K. This coincides with the T_{CDW2} observed at ambient pressure, and confirms the role of the lattice structure in the emergence of CDW transition [7]. In the case of $LaAuSb_2$, it exhibited the CDW transition at 83 K. However, it is noted that a lattice parameter modulation leading to the CDW initiates at 250 K, which is associated with the formation of FS nesting [1]. Both $EuBiS_2F$ [8] and $LaPt_2Si_2$ [9] showed similar lattice parameter variations and CDW transitions.

In electronic band calculations, Dirac points were observed in $LaTMSb_2$ (TM = Cu, Ag, Au) [10] and similar phenomena has been observed in several topological insulators (TIs) [11], graphene [12] and Fe-based superconductors ($BaFe_2As_2$) [13]. $LaAgSb_2$ showed a strong two-dimensionality [14] of the FS up to 3.5 GPa [6,10]. However, $LaCuSb_2$ shows three-dimensionality in the FS and $LaAuSb_2$ shows intermediate nature. In $LaTMSb_2$, conduction electrons are mainly from the Sb-5p electrons. However, TM-d electrons also play a significant role. $LaAgSb_2$ exhibits two-hole FS, and both $LaAuSb_2$ and $LaCuSb_2$ showed a single hole FS [10]. We also note that

This article is part of the Special issue on 'High pressure materials science: recent trends'.

Published online: 27 September 2022

the angle-resolved photoemission spectroscopy revealed the presence of Dirac cone-like structure in $LaAgSb_2$ due to the crossing of the bands located along the Γ-M direction [15]. Similar band crossing and Dirac-cone-like structure were observed in $LaAuSb_2$ [1]. Interestingly, the calculated total electronic density of states for both $LaAgSb_2$ [15] and $LaAuSb_2$ [1] are found to be very similar. On the other hand, from the DFT point of view, calculations predicted that the $LaAuSb_2$ retain its tetragonal structure (P4/nmm) up to 150 GPa, with only a volume collapse above 100 GPa [1]. All these observations underline the role of lattice degrees of freedom in determining the electronic phenomena in these ternary antimonides. To further appreciate these aspects here we discuss the ambient pressure Raman mode response of $LaTMSb_2$ (TM = Au and Ag) and compare the pressure response of the lattice structure.

We have earlier reported a complete suppression of the CDW transition in $LaAuSb_2$ at a critical pressure of 3.6 GPa [1]. However, there is no structural phase transition in $LaAuSb_2$ associated with the suppression of the CDW. Our synchrotron XRD data reveal the structure to be stable up to 12.2 GPa, the maximum pressure explored in our study. A SC transition with T_c = 0.6 K at ambient pressure is observed in this system [3]. Interestingly, hydrostatic pressure is found to increase the T_c up to 1.05 K for a moderate pressure of 0.64 GPa [3]. In case of $LaAgSb_2$, SC had not yet been reported [16–18]. Interestingly, both CDW transitions decreased under pressure, with a rate of $dT_{CDW1}/dP \sim -51$ K GPa^{-1} and $dT_{CDW2}/dP \sim -80$ K GPa^{-1} [16]. On the other hand, magnetoresistance measurements under pressure reveal the complete suppression of the same at 21.5 GPa, where there is also a subtle structural rearrangement [19]. An earlier powder XRD measurements under high pressure in this system revealed a mixed tetragonal (P4/nmm, No. 129) and distorted monoclinic structure (space group P112/n) at $P = \sim 4$ GPa with a corresponding

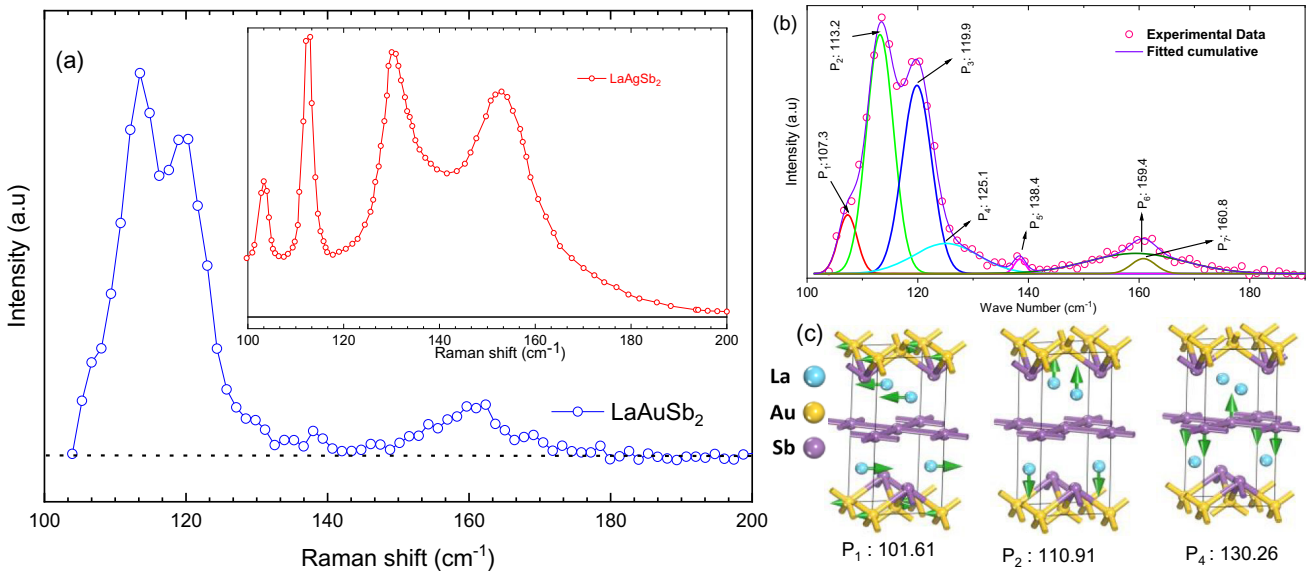

Figure 1. (**a**) Observed Raman spectrum of $LaAuSb_2$. Inset represents a digitized figure of $LaAgSb_2$ Raman data (courtesy: Singha *et al* [7]). (**b**) Observed (pink circles) and fitted Raman spectrum (violet line) of $LaAuSb_2$. Fitting was done considering the calculated DFT Raman modes (refer table 1). (**c**) Pictorial view of the vibrational sequence for three selected Raman modes.

Table 1. $LaTSb_2$ (Ag, Au) single-crystal DFT and experimental Raman modes comparison.

	$LaAgSb_2$ [7]		$LaAuSb_2$	
	DFT (cm^{-1})	Experimental (cm^{-1})	DFT (cm^{-1})	Experimental (cm^{-1})
P0	E_g^1 32.78	—	E_g^1 20.19	—
P1	E_g^2 62.93	82	E_g^2 53.99	—
P2	B_{1g}^1 99.19	92	B_{2g}^1 89.89	—
P3	E_g^3 100.11	99	E_g^3 101.61	107.33
P4	B_{1g}^2 105.12	109	$A_{1g}^1$110.91	113.18/119.85
P5	A_{1g}^1 108.21	127	B_{2g}^2 130.26	125.1
P6	A_{1g}^2 121.59	132	A_{1g}^2 136.37	138.43
P7	E_g^4 162.65	151	E_g^4 157.36	159.42/160.77

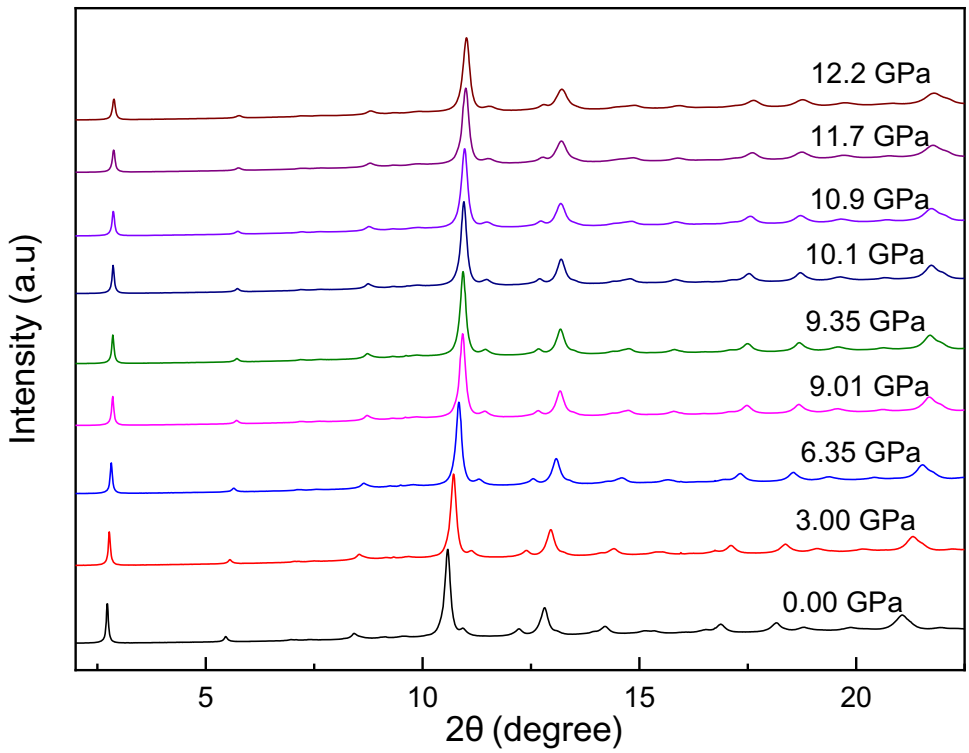

Figure 2. Measured high-pressure XRD spectrum of $LaAuSb_2$ under various pressures. Patterns are shifted vertically to improve presentation clarity.

noticeable drop in the Raman $A_1{}^{1g}$ mode intensity [7]. As a result of the pressure-dependent XRD and Raman measurements, the suppression of CDW transition is associated to a structural reordering. In fact, in $LaAuSb_2$ also there is a very subtle structural rearrangement associated with the suppression of the CDW with pressure [1]; however, the effect is much less marked, compared to $LaAgSb_2$ in pressure-induced suppression of the CDW [7] or magnetoresistance [19]. These interesting observations reveal the importance of the TM site occupant in $LaTMSb_2$ in the CDW, magnetoresistance, SC and similar phenomena.

2. Methods

2.1 *Experimental*

The self-flux method was used to synthesize the $LaAuSb_2$ single crystals from a 1:2:20 mixture of La (99.9%), Au (99.9%) and Sb (99.9%), and reference [20] contains a detailed description of the synthesis procedures. Pressure-dependent powder XRD data were collected at the Xpress beamline of the Elettra Synchrotron Center, Trieste, Italy [21]. A PACE5000-based automatic membrane drive was used in combination with a membrane-driven symmetric Diamond anvil cell (DAC). The pressure-transmitting medium used was a 4:1 methanol–ethanol (ME) mixture. The *in-situ* Ruby florescence technique has been used to measure the pressure inside the DAC, and 10 μm ruby chips were loaded along with the sample for this purpose. A monochromatic circular beam with a wavelength of 0.4957 Å and a cross-sectional diameter of 40 μm were used to collect high-pressure diffraction data, and Pilatus3S-6M large-area detector was used for data collection. By the use of FIT2D software, collected data were converted into intensity *vs.* 2θ plots. The Rietveld method was used to refine the structural model using the GSAS II suite. Using a 532 nm (green) diode laser with 2400 l mm^{-1} gratings at ambient pressure, Raman scattering measurements were done in a specialized Renishaw Raman confocal microscope available at the Xpress beamline. Reference [22] contains a detailed description of the data collection process from Raman spectrum.

2.2 *Computational methods*

Total energies have been calculated by the projected augmented plane-wave implementation of the Vienna Ab initio Simulation Package (VASP) [23,24]. All these calculations were made using the Perdew–Burke–Ernzerhof [25] exchange-correlation functional with 2050 k points in the Brillouin zone with a 600 eV plane-wave cutoff. Ground-state geometries were determined by minimizing both the stresses and the Hellman–Feynman forces using the conjugate-gradient algorithm with a force convergence threshold of 10^{-3} eV $Å^{-1}$. The Raman active modes are calculated with Raman off-resonant activity calculator using VASP as a back-end [26].

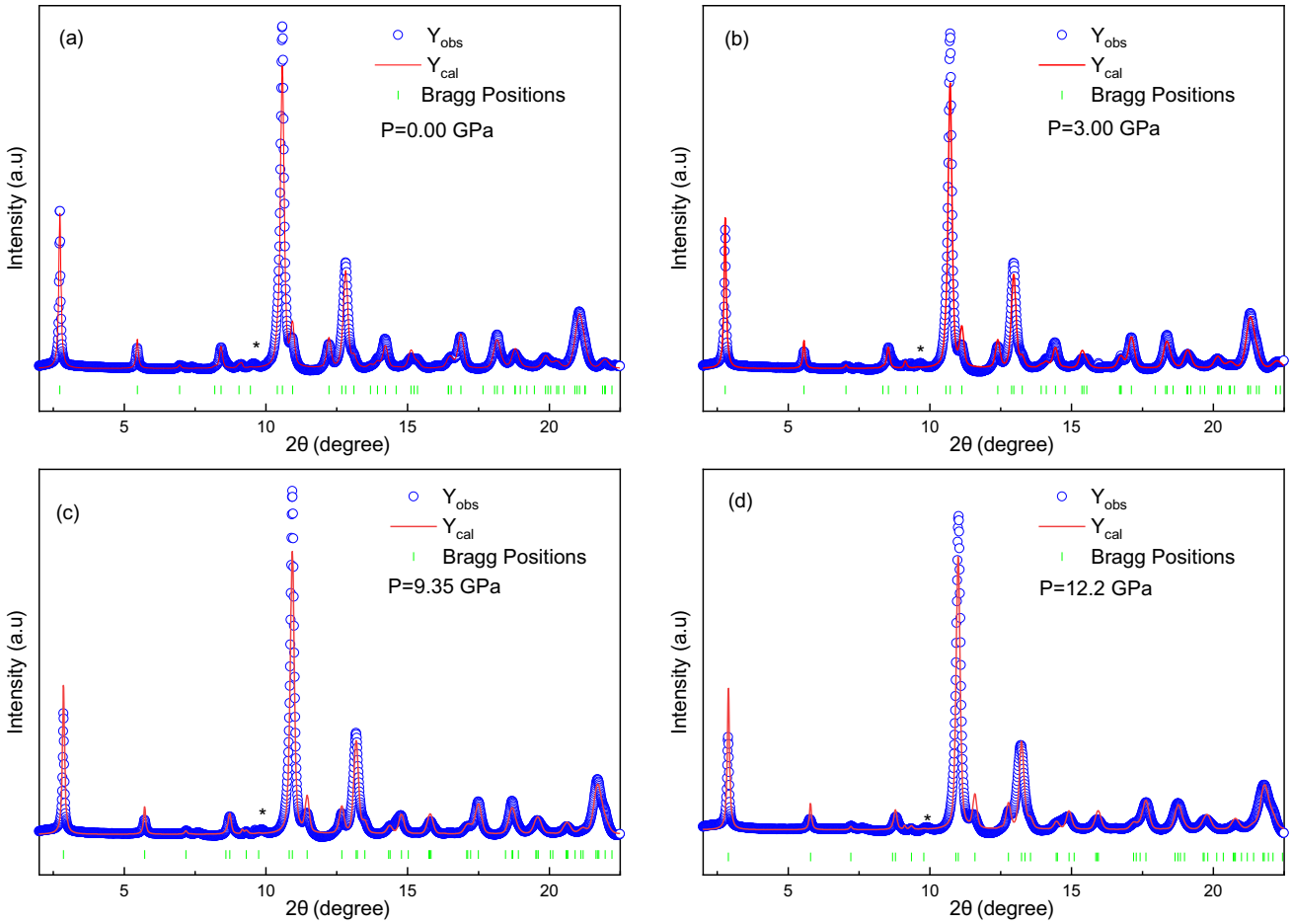

Figure 3. Measured X-ray diffraction patterns of $LaAuSb_2$ sample at ambient temperature and (**a**) 0.00, (**b**) 3.00, (**c**) 9.35 and (**d**) 12.2 GPa together with the Rietveld refinement results (solid red lines). The Bragg peak positions are indicated by green vertical bars below the diffractogram, and the Sb impurity peaks are indicated by *.

3. Results and discussion

3.1 *Raman results and comparison*

Figure 1a shows the measured Raman spectrum of $LaAuSb_2$. Measured Raman spectra of $LaAgSb_2$ reported in reference [7] is shown here as an inset. A deconvolution of the measured Raman spectra is undertaken considering the DFT results (refer table 1). A similar spectral deconvolution of the $LaAgSb_2$ is also presented in reference [7]. We have observed seven Raman modes in the range of 100–200 cm^{-1} (107.3, 113.2, 119.9, 125.1, 138.4, 158.4 and 160.8 cm^{-1}) for our $LaAuSb_2$ sample. We found four E_g (20.19, 53.99, 101.61, 157.36 cm^{-1}), two B_{2g} (89.89, 130.26 cm^{-1}) and two A_{1g} (110.91, 136.37 cm^{-1}) modes from the DFT calculation. Table 1 compares the Raman modes observed from the experiment and DFT for both $LaAgSb_2$ and $LaAuSb_2$. We note that the DFT method used in reference [7] for the identification of the Raman modes is similar as in the current work. It is found that the Raman spectra for both samples are similar. We note that the low frequency modes in our case were missing due to the instrument limitation (notch filter cut-off for frequencies below 100 cm^{-1}).

3.2 *High-pressure XRD results and comparison*

Figure 2 shows the measured high-pressure XRD spectrum of $LaAuSb_2$ under various pressures. To improve presentation clarity, XRD patterns are positioned vertically. Previously, we have done a pressure-dependent synchrotron XRD measurements twice for $LaAuSb_2$ using a silicone oil (first run up to 7 GPa) and ME (second run up to 9 GPa) as a pressure-transmitting medium. In both runs, we have not observed any structural transitions [1]. The data presented in figure 2 are from a third run. From these high-pressure XRD runs, we do not observe any new peaks implying the absence of any structural anomaly up to 12.2 GPa. Recently, Singha *et al* [7] reported the pressure effect on the structure of $LaAgSb_2$. They found mixed tetragonal and monoclinic phases from 4 to 9 GPa, followed by a mixed monoclinic and orthorhombic phase in higher pressures. These interesting results stimulate us to redo the structural

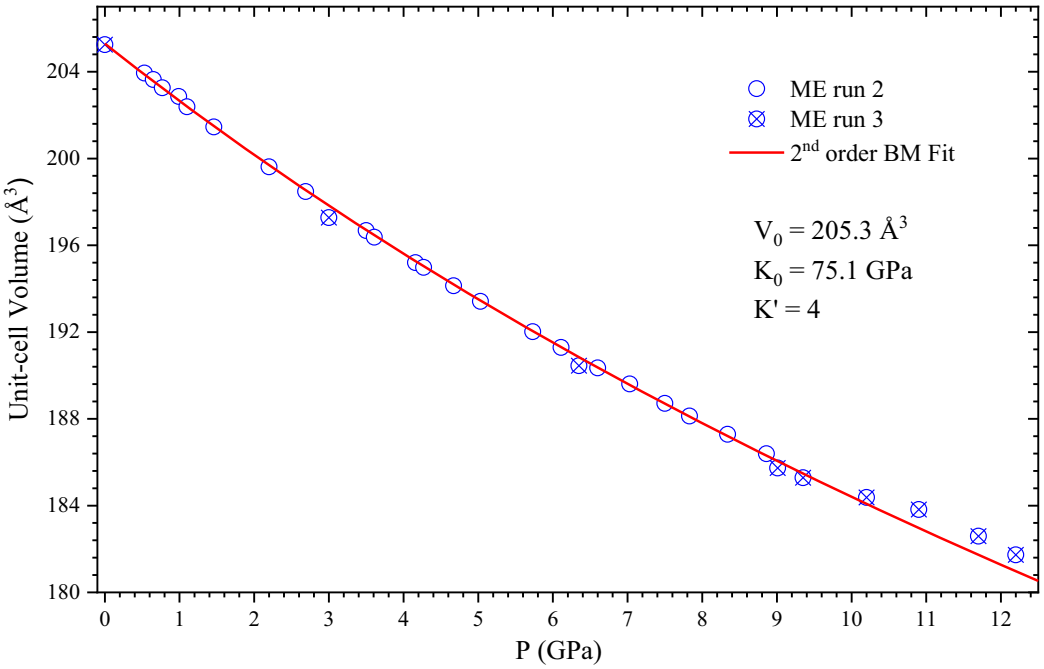

Figure 4. A unit-cell volume as a function of pressure. Data corresponding to ME run 2 is from earlier study (open circles) [1]. Crossed out circle data are from 3rd ME high-pressure XRD run. The solid red line is the result of fitting the data with a second-order Birch–Murnaghan equation of state (see text for details).

measurements on $LaAuSb_2$, so we have done pressure measurement up to 12.2 GPa and it differs from the results reported by Singha *et al* [7].

Figure 3 presents examples of the structural refinement results of the high-pressure XRD data. As is evident, the data at different pressures are well fitted with a $ZrCuSi_2$-type tetragonal structure with a space group of P4/nmm. See figure 1c for the visualization of the $ZrCuSi_2$-type tetragonal structure of $LaAuSb_2$. The estimated lattice parameters at ambient pressure are a = 4.44215 Å and c = 10.4015 Å, which are similar to those already reported [1,20]. It is to be noted that our samples contained a small amount of the Sb impurity phase. These impurity peaks are indicated in the spectra in figure 3 by *.

Figure 4 shows a pressure dependence of the unit-cell volume at ambient temperature. In this plot, we have used the data from the two pressure runs (2 and 3) involving the 4:1 ME as a pressure-transmitting medium. The equation of state fit provides the unit-cell volume of 205.31 $Å^3$ at ambient pressure and the bulk modulus (K_0) of 75.1 GPa, with the pressure derivative of K = 4 (fixed). Our calculated bulk modulus from DFT for $LaAuSb_2$ is 74 GPa, which has an excellent agreement with the experimentally obtained one (75.1 GPa). The equation of state fit of $LaAgSb_2$ with the fixed pressure derivative of K = 4 showed the tetragonal phase to have a bulk modulus of 67.5 GPa from reference [7] and 84.3 GPa from reference [20]. Incidentally, bulk modulus of 74 GPa was reported from the equation of state fit with pressure derivative of K = 4.8 [17].

4. Conclusion

In this article, we have presented the experimental Raman spectroscopy results of the $LaAuSb_2$ and $LaAgSb_2$ systems to further underline the structural similarity of these ternary antimonides. Further, we have used DFT calculations to interpret the experimental Raman data of $LaAuSb_2$ thus revealing the mode characterizations. We have further undertaken a systematic high-pressure synchrotron powder XRD study of $LaAuSb_2$. Our experimental data rule out any structural phase transitions in this system up to 12.2 GPa. Compared to this, the isostructural sister compound $LaAgSb_2$ showed a structural phase transition at 4 GPa. This structural phase transition is responsible for the suppression of CDW transition in $LaAgSb_2$. Interestingly, although there is no symmetry changing structural phase transitions associated with the pressure-dependent suppression of the CDW in $LaAuSb_2$, the lattice parameters revealed a slope change at the critical pressure, underlining a clear role of lattice also in this system in suppressing the CDW [1]. Thus, taken together, our results underline an intimate role of the lattice structure in governing the CDW phenomena in the ternary antimonides $LaTMSb_2$ (TM = Au or Ag).

Acknowledgements

We thank Xpress beamline of the Elettra Sincrotrone Trieste for beamtime. GL gratefully acknowledges the receipt of a fellowship from the ICTP Programme for Training and Research in Italian Laboratories, Trieste, Italy. BJ acknowledges the availability of DACs through Xpress-PLUS internal project of Elettra Sincrotrone Trieste. PV gratefully acknowledges the Research Council of Norway for providing the computer time (under Projects No. NN2875k and No. NS2875k) at the Norwegian supercomputer facility. AS wishes to thank DST (MES, and SERB), UGC-DAE-CSR (Indore), MHRD-RUSA, TANSCHE (Chennai) and BRNS (Mumbai) for financial support.

References

[1] Lingannan G, Joseph B, Vajeeston P, Kuo C N, Lue C S, Kalaiselvan G *et al* 2021 *Phys. Rev. B* **103** 195126
[2] Song C, Park J, Koo Lee K B, Rhee J Y, Bud'ko S L *et al* 2003 *Phys. Rev. B* **68** 035113
[3] Du F, Su H, Luo S S, Shen B, Nie Z Y, Yin L C *et al* 2020 *Phys. Rev. B* **102** 144510
[4] Inada Y, Thamizhavel A, Yamagami H, Takeuchi T, Sawai Y, Ikeda S *et al* 2002 *Philos. Mag. B* **82** 1867
[5] Balicas L, Nakatsuji S, Lee H, Schlottmann P, Murphy T P and Fisk Z 2006 *AIP Conf. Proc.* **850** 693
[6] Akiba K, Umeshita N and Kobayashi T C 2022 *Phys. Rev. B* **105** 035108
[7] Singha R, Samanta S, Bhattacharya T S, Chatterjee S, Roy S, Wang L *et al* 2020 *Phys. Rev. B* **102** 205103
[8] Zhai H F, Tang Z T, Jiang H, Xu K, Zhang K, Zhang P *et al* 2014 *Phys. Rev. B* **90** 064518
[9] Falkowski M, Doležal P, Andreev A V, Duverger-Nédellec E and Havela L 2019 *Phys. Rev. B* **100** 064103
[10] Hase I and Yanagisawa T 2014 *Phys. Procedia* **58** 42
[11] Hasan M Z and Kane C L 2010 *Rev. Mod. Phys.* **82** 3045
[12] Neto A C, Guinea F, Peres N M, Novoselov K S and Geim A K 2009 *Rev. Mod. Phys.* **81** 109
[13] Richard P, Nakayama K, Sato T, Neupane M, Xu Y M, Bowen J H *et al* 2010 *Phys. Rev. Lett.* **104** 137001
[14] Wang K and Petrovic C 2012 *Phys. Rev. B* **86** 155213
[15] Shi X, Richard P, Wang K, Liu M, Matt C E, Xu N *et al* 2016 *Phys. Rev. B* **93** 081105(R)
[16] Akiba K, Nishimori H, Umeshita N and Kobayashi T C 2021 *Phys. Rev. B* **103** 085134
[17] Bud'ko S L, Wiener T A, Ribeiro R A, Canfield P C, Lee Y, Vogt T *et al* 2006 *Phys. Rev. B* **73** 184111
[18] Torikachvili M S, Bud'ko S L, Law S A, Tillman M E, Mun E D and Canfield P C 2007 *Phys. Rev. B* **76** 235110
[19] Zhang B, An C, Chen X, Zhou Y, Zhou Y, Yuan Y *et al* 2021 *Chinese Phys. B* **30** 076201
[20] Kuo C N, Shen D, Li B S, Quyen N N, Tzeng W Y, Luo C W *et al* 2019 *Phys. Rev. B* **99** 235121
[21] Lotti P, Milani S, Merlini M, Joseph B, Alabarse F and Lausi A 2020 *J. Synchrotron Radiat.* **27** 222
[22] Lingannan G, Joseph B, Sundaramoorthy M, Kuo C N, Lue C S and Arumugam S 2022 *J. Phys.: Condens. Matter* **34** 245601
[23] Kresse G and Furthmüller J 1996 *Phys. Rev. B* **54** 11169
[24] Kresse G and Furthmüller J 1996 *Comput. Mater. Sci.* **6** 15
[25] Perdew J P, Burke K and Ernzerhof M 1997 *Phys. Rev. Lett.* **78** 1396
[26] Fonari A and Stauffer S 2013 https://github.com/raman-sc/VASP/